**Atmospheric
Chemistry
and Physics
Discussions**

ACPD

3, 4943–4988, 2003

OIO homogeneous
nucleation

J. B. Burkholder et al.

Title Page

Abstract	Introduction
Conclusions	References
Tables	Figures

◄◄	►►
◄	►
Back	Close

Full Screen / Esc

Print Version

Interactive Discussion

© EGU 2003

Laboratory studies of the homogeneous nucleation of iodine oxides

J. B. Burkholder[1], J. Curtius[1, *], A. R. Ravishankara[1, **], and E. R. Lovejoy[1]

[1]Aeronomy Laboratory, National Oceanic and Atmospheric Administration, 325 Broadway, Boulder, CO 80305-3328, USA
*now at: Institute for Atmospheric Physics, Mainz University, Mainz, Germany
**also associated with the Dept. of Chemistry and Biochemistry, U. of Colorado, Boulder, CO 80309, USA

Correspondence to: J. B. Burkholder (burk@al.noaa.gov)

Abstract

Laboratory experimental results of iodine oxide nucleation are presented. Nucleation was induced following UV photolysis of CF_3I or CH_2I_2 in the presence of excess ozone. Measurements were performed in a 70 L Teflon reactor with new particles detected using an Ultrafine Condensation Particle Counter, UCPC. The experimental results are interpreted using a coupled chemical – aerosol model to derive model parameters assuming single component homogeneous nucleation of OIO. The aerosol model results have been applied in an atmospheric box-model to interpret the possible implications of iodine oxide nucleation in the marine boundary layer. The model calculations demonstrate that IO and OIO concentrations reported in recent field measurements (Allan et al., 2000, 2001) are not sufficient to account for significant aerosol production either in the coastal or open ocean marine boundary layer using the mechanism presented. We demonstrate that inhomogeneous sources of iodine oxides, i.e. "hot" spots with elevated iodine species emissions, could account for the aerosol production bursts observed in the coastal region near Mace Head, Ireland.

1. Introduction

The impact of new particle formation in the troposphere on climate, both regional and global, is a topic of great interest. Sulfur chemistry probably plays an important role in new particle formation through either the H_2SO_4/H_2O or $H_2SO_4/NH_3/H_2O$ chemical systems. However, recent field studies have observed particle formation possibly related to iodine chemistry in the marine environment (O'Dowd et al., 2002 and references within) and volatile organic compounds (VOCs) in remote forested regions (Marti et al., 1997; Kavouras et al., 1998, 1999; Leaitch et al., 1999). The evaluation and impact of these sources of new particles is currently an active area of atmospheric research.

To date, the 1998–1999 PARFORCE campaign at Mace Head station on the western

coast of Ireland (O'Dowd et al., 2002) is one of the most comprehensive field studies of "new" particle formation in the coastal marine environment. During this campaign, dramatic nucleation events were observed which yielded particle concentrations as high as 10^6 cm^{-3} for durations of hours under certain conditions. The nucleation mecha-

5 nism has not been definitively identified but the correlation with both solar flux and low tide and the identification of iodine oxides in the particles has lead to the proposal that alkyl iodides (particularly CH_2I_2) that are emitted by macroalgae are precursors for new particle formation (Carpenter et al., 1999 and references within).

Hoffmann et al. (2001) and Jimenez et al. (2003) have evaluated the hypothesis that

10 alkyl iodides are responsible for the observed nucleation events through a series of laboratory experiments. In these experiments, $CH_2I_2/O_3/$Air mixtures were photolyzed in the near UV and the formation of ultra-fine particles measured. Their experiments and results from kinetic studies reported in the literature lead Hoffmann et al. (2001) to suggest the following reaction mechanism to explain new particle formation

15 $$CH_2I_2 + h\nu \rightarrow CH_2I + I \tag{1}$$

$$I + O_3 \rightarrow IO + O_2 \tag{2}$$

$$IO + IO \rightarrow OIO + I \tag{3}$$

$$OIO + OIO \leftrightarrow I_2O_4 \tag{4}$$

$$I_2O_4 + OIO \leftrightarrow\leftrightarrow\leftrightarrow \text{``}particle\text{''}, \tag{5}$$

20 where Reaction (5) represents multiple OIO addition steps leading to the formation of a stable iodine oxide cluster. In this mechanism, aerosol formation results from single component homogeneous nucleation of OIO. The OIO molecule has been rather elusive in the laboratory such that its physical properties are currently unknown while its reactivity and photochemical properties (Ingham et al., 2000; Ashworth et al., 2002)

25 are topics of current study.

Although the particle formation mechanism awaits verification, Hoffmann et al. (2001) have demonstrated that UV photolysis of CH_2I_2 and O_3 gas mixtures do indeed lead to iodine oxide particle formation. Jimenez et al. (2003) have subsequently extended the laboratory studies of Hoffmann et al. to include a range of CH_2I_2 concentrations nearer to that observed in the marine boundary layer (MBL). Jimenez et al. used a suite of particle analysis instrumentation to evaluate the particle composition and physical properties. The particle growth was well characterized and the particles were shown to contain mainly iodine oxides. Their work supports the particle formation mechanism proposed by Hoffmann et al. (2001).

In spite of the work of Hoffmann et al. (2001) and Jimenez et al. (2003), the ability to predict and model the iodine oxide homogeneous nucleation process in the atmosphere is still limited. A physically based parameterization of the nucleation process, which in turn can be applied, under atmospheric conditions, is needed. In this work, we have extended the laboratory measurements on the iodine oxide nucleation system through variation of critical experimental parameters to better evaluate the nucleation process. A kinetic nucleation model is presented and used to interpret the experimental observations and derive parameters that are applicable for atmospheric model calculations.

2. Experimental details

In this work, we have evaluated the iodine chemistry induced homogeneous nucleation by interpreting laboratory chamber measurements made under a range of controlled conditions. The conditions varied in these experiments include the initial iodine precursor concentrations, the iodine precursor molecule, photolysis rate coefficients, duration of photolysis, and temperature. For each set of experimental conditions, the time dependence of the ultra-fine aerosol particles formed was measured and interpreted using a coupled gas phase reaction mechanism and nucleation model.

Our experimental approach is similar in principle to that employed in the recent lab-

OIO homogeneous nucleation

J. B. Burkholder et al.

◄◄ | ►►

◄ | ►

Back | Close

Full Screen / Esc

Print Version

Interactive Discussion

oratory studies by Hoffmann et al. (2001) and Jimenez et al. (2003). Our work is complementary to these studies but has an emphasis on a physical (thermodynamic) description of the elementary steps in the homogeneous nucleation process. An accurate physical description of the nucleation will enable modeling homogeneous nucleation and aerosol formation under conditions relevant to the atmosphere.

A diagram of the experimental apparatus is given in Fig. 1. The apparatus consists primarily of the following four components; (1) a Teflon bag reactor, (2) an Ultra-fine Condensation Particle Counter, UCPC, (3) fluorescent photolysis lamps, and (4) a gas handling manifold. The details and operation of each of these components is described separately below.

2.1. Teflon bag reactor

The Teflon bag reactor was made from 5 mil thick FEP Teflon ($24'' \times 36''$, flat dimensions) with welded seams on three edges. The fourth edge (along the $24''$ dimension) was sealed with a removable compression clamp to allow access to the bag interior. The bag was suspended vertically from the compression clamp and had a diameter at the center of ~40 cm at full inflation (internal pressure 5 Torr over ambient pressure, 623 Torr). Vacuum fittings made of PFA with Viton O-ring seals were mounted near the top, center and bottom of the bag. The top fitting was used for the aerosol sampling line ($1/4''$ o.d. Teflon tubing; 50 cm long) from the UCPC. This configuration enabled the sampling line to remain stationary in the center of the bag while the bag collapsed during the course of an experiment.

The initial reactant concentrations in the bag were calculated from the measured pressures in the vacuum manifold and the volume of the bag when fully inflated (i.e. the gas phase concentrations of the compounds and reaction intermediates in the bag were not directly measured). The volume of the bag at full inflation was determined experimentally by calibrated expansions to be 72 ± 1.5 L. The vacuum manifold was made of Pyrex with Teflon valves. The manifold was used to measure and introduce the samples into the Teflon bag reactor. Pressures of the dilute reactant gas mixtures

were measured with 10 and 1000 Torr capacitance manometers. A small calibrated volume, 86 cm^3, was attached to the manifold and used to quantify the amount of reactant flushed into the Teflon bag reactor.

Dilute gas phase mixtures of the reactants were introduced into the bag separately through the center inlet of the bag. The experimental results were independent of the order with which the reactants were added to the bag. The gases were found experimentally to be well mixed during the filling of the bag, a procedure that took ∼5 min. The reactor bag was flushed between experiments by (1) pumping out the contents until the bag collapsed onto itself, (2) fully inflating the bag with clean N$_2$ or Air and (3) pumping out the contents again. This sequence was repeated three times. Further, background experiments with O$_3$ and Air but no iodine precursor were then performed to confirm cleanliness, i.e. no background particle production on the time scale of our experiments, ∼1000 s. The O$_3$/Air mixture was flushed from the bag using the steps outlined above.

The optical transmission of the Teflon bag over the wavelength range 300–400 nm was measured to vary smoothly from ∼70% to 85%. The transmission of the Teflon did not change over the course of the experiments.

2.2. Ultra-fine Condensation Particle Counter

A commercial Ultra-fine Condensation Particle Counter, UCPC, (TSI Inc., model 3025A)[1] was used to measure particle production in our experiments. The minimum size cut-off for spherical particles of the UCPC is quoted by the manufacturer to be 3 nm (50% detection efficiency). The UCPC has a maximum measurable particle density of 1×10^5 particle cm^{-3}. In our experiments, particle concentration measurements

---

[1]Certain commercial equipment, instruments, or materials are identified in this article in order to adequately specify the experimental procedure. Such identification does not imply recognition or endorsement by the National Oceanic and Atmospheric Administration, nor does it imply that the material or equipment identified are necessarily the best available for the purpose.

were made under "high" flow, 1500 cm^3 min, conditions without dilution of the sample flow while using the dynamic signal averaging algorithm of the UCPC.

The contents of the bag were sampled through 50 cm of 1/4″ o.d. Teflon tubing that was isolated from the UCPC by a 1/4″ straight bore valve at the instrument inlet. Particle loss in the sampling line was determined to be negligible, < 5%, when using the "high" flow rate sampling mode of the UCPC. The UCPC sampled the contents of the bag continuously during an experiment.

In several experiments, a nano-differential mobility analyzer (nDMA, TSI Inc. Model 3085) was used to evaluate the particle size distribution. Replicate nucleation experiments were conducted under identical initial conditions while selecting 3, 5, 8, 10, and 15 nm diameter particles.

2.3. Photolysis lamps

Fluorescent black lamps were used to initiate the iodine gas phase chemistry through the photolysis of iodine containing precursor molecules (CH_3I, CH_2I_2 or CF_3I) in the presence of excess ozone. Experiments were performed using two different types of blacklamps (BLB365 or BL350, 40 W lamps, 48″ long) with different spectral outputs. The spectral output of the lamps and the UV spectra of CH_2I_2 and CF_3I are shown in Fig. 2. The BLB365 (BLB: black light blue) lamp emits between 350 and 400 nm with peak intensity at 365 nm. The BLB365 lamps have weak emission at the 404 and 435 nm (Hg transitions) but no significant emission in the visible or UV regions. The BL350 lamp emits between 300 and 400 nm with peak intensity at 350 nm. The BL350 lamps have stronger 404 and 435 nm Hg line emission but also have no significant emission in the visible or UV regions. Twelve pairs of photolysis lamps were mounted around the perimeter of the reactor ~10 cm from the surface of the fully inflated Teflon bag, Fig. 1. Based on the lamp geometry the light flux inside the bag was calculated to be uniform to within ~20% and was brightest at the bag surface.

The average photolysis lamp flux (within the reactor bag) was experimentally deter-

mined using CH_2I_2 as an actinometer. The loss of CH_2I_2 during photolysis with the BLB365 lamps was monitored by UV absorption (254 nm) in an externally mounted 50 cm long cell. The contents of the reactor bag were continuously circulated through the absorption cell during the calibration measurement which took ~30 min. The CH_2I_2 photolysis rate coefficient (i.e. CH_2I_2 loss rate coefficient) was measured to be $(1.25 \pm 0.05) \times 10^{-3}\,s^{-1}$. A CF_3I photolysis rate coefficient with the BL350 lamps of $3.3 \times 10^{-5}\,s^{-1}$ was calculated using the measured CH_2I_2 photolysis rate coefficient and the relative spectral overlap with the photolysis lamps. These BL350 lamps photolysis rate coefficients for CH_2I_2 and CF_3I are approximately a factor of five greater than the values found in the atmosphere. (Roehl et al., 1995 and Solomon et al., 1994) The photolysis rate coefficients for ozone, I_2, IO, and OIO were calculated relative to the experimentally measured CH_2I_2 value and are given in Table 1. We estimate the uncertainty in the calculated CF_3I photolysis rate coefficient to be 25%.

Photolytic loss of ozone is not significant in the presence of an atmosphere of air due to its rapid regeneration, $O + O_2 + M \rightarrow O_3 + M$. The I_2 photolysis rate coefficient is on the same time scale as the nucleation experiments and is therefore included in the chemical mechanism described below. The IO photolysis rate coefficient is rather high, $0.18\,s^{-1}$, due to its large absorption cross section between 350 and 400 nm. The photolysis rate coefficient of OIO is highly uncertain due to uncertainties in both its absorption cross section (Bloss et al., 2001) and quantum yields (Ingham et al., 2000; Ashworth et al., 2002). However, using reasonable values for the OIO absorption cross sections and a unit quantum yield results in a small photolysis rate coefficient with either of the BL350 or BLB365 lamps used. As will be shown in the Results and Discussion section, the photolytic loss of OIO will not significantly influence our interpretation of the nucleation experiments provided the photolysis rate coefficient of OIO is less than $0.01\,s^{-1}$.

2.4. Materials and sample handling

Samples of CH_2I_2, CH_3I, CF_3I, and synthetic air (21% O2, 79% N2) were used without purification. Upper limits for the I_2 impurity in the CH_2I_2, CH_3I, and CF_3I samples was determined by UV/vis absorption measurements of the pure compounds to be < 0.01%, < 0.07%, and < 0.0001%, respectively. The hydrocarbon impurity in the synthetic air was determined to be less than 1 ppb by gas chromatographic analysis. The H_2O impurity of the synthetic air cylinder was quoted to be < 5 ppm.

Dilute gas mixtures of CH_2I_2, CF_3I, CH_3I and O_3 in synthetic air were prepared and stored in individual 12 L blackened Pyrex bulbs. The mixing ratios of these compounds in the bulbs were determined by UV absorption using either a 100 or 25 cm long cell and a diode array spectrometer. Periodic UV absorption measurements confirmed the sample stability, ±3%, over the course of the experiments.

The Teflon bag reactor was nominally operated at room temperature. A fan mounted at the base of the experimental apparatus but outside the Teflon bag, dissipated the heat generated by the photolysis lamps. Typically, the temperature of the reactor increased $\sim 2°$ C during the course of an experiment. Several nucleation experiments were also performed at elevated temperatures, $\sim 45 \pm 5°$ C, by enclosing the reactor and externally heating the surrounding air with a space heater.

3. Gas phase chemical reaction mechanism and homogeneous nucleation model

3.1. Gas phase chemical reaction mechanism

The interpretation of our experimental measurements employed a coupled gas phase chemical reaction mechanism and homogeneous nucleation model. The reaction mechanism, rate coefficients, and product yields used in the chemical mechanism are given in Table 2. The iodine precursor photolysis rate coefficients are given in Table 1.

Title Page

Abstract	Introduction
Conclusions	References
Tables	Figures

◄◄　►►

◄　►

Back　Close

Full Screen / Esc

Print Version
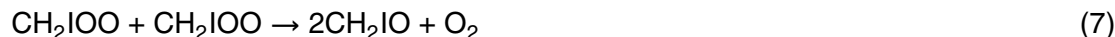
Interactive Discussion

The photolysis rate coefficient was also varied in several experiments by changing the number of lamps used. There have been several rate coefficient and product yield measurements for the IO + IO reaction (Harwood et al., 1997; Bloss et al., 2001). However, despite this effort our understanding of the reaction products and their yields is still incomplete. In the present work it is assumed that OIO is the species responsible for the observed nucleation and therefore its yield in the IO + IO reaction, 0.30 (Bloss et al., 2001) is of primary importance.

The formation and fate of the other IO + IO reaction products (I, I_2, IOI, and I_2O_2) are accounted for as follows. The yield of I atoms, Reaction (3a), is relatively small. I atoms will be rapidly converted back to IO via Reaction (2). The yield of I_2, Reaction (3b), is also relatively small, ~0.05. However, the formation of I_2 represents a small sink for reactive iodine because of the relatively slow I_2 photolysis in our apparatus. IOI has not been identified as a reaction product in the IO self-reaction and is assumed to be zero in our analysis. It is assumed that the IO dimer, I_2O_2, represents the balance of the reaction products. The chemical properties of I_2O_2 are currently unknown but by analogy with the chlorine and bromine dimers, Cl_2O_2 and Br_2O_2, it is expected to be thermally unstable at room temperature (Sander et al., 2002). I_2O_2 is therefore expected to rapidly decompose back to IO radicals at room temperature and represent a null cycle with respect to the IO radical concentration.

Reaction (1), the photolysis of CH_2I_2, produces I and CH_2I radicals as products. The CH_2I radical can release the second iodine atom via the following sequence of reactions.

$$CH_2I + O_2 \rightarrow CH_2IOO \qquad (6)$$

$$CH_2IOO + CH_2IOO \rightarrow 2CH_2IO + O_2 \qquad (7)$$

$$CH_2IO \rightarrow CH_2O + I. \qquad (8)$$

Both Reactions (6) and (8) are expected to be rapid and for our purposes are instantaneous while Reaction (7) is rate limiting. The rate coefficient for Reaction (7) has not

been reported but we expect k_7 to be similar to that of the CH_3OO radical self-reaction, 4.7×10^{-13} cm^3 molecule^{-1} s^{-1} (Sander et al., 2002). Our over simplified chemical model used in the analysis of experiments using CH_2I_2 does not treat the CH_2I radical explicitly but assumes an immediate release of the I atom.

5   Although previous laboratory measurements (Hoffmann et al., 2001; Jimenez et al. 2003) have exclusively used CH_2I_2 as the iodine precursor, we have used CF_3I as the I atom precursor for the bulk of the measurements for the reasons outlined below. First, CF_3I contains a single I atom which is released upon photolysis and therefore represents a "cleaner" and better characterized I atom source than CH_2I_2. Second,

10   due to the significant differences in photolysis rate coefficients (Table 1), CF_3I yields a nearly constant iodine atom production rate over the duration of the measurements, ~1000 s, while CH_2I_2 is significantly depleted over this time period. The CF_3I purity is sufficiently high, i.e. low I_2 impurity, that background aerosol production was not observed when high concentrations of CF_3I were used. CF_3I therefore represents a

15   well characterized I atom source. Finally, the high vapor pressure of CF_3I, > 1 atm., makes handling the samples and flushing the Teflon bag more efficient than for CH_2I_2, ~2 Torr vapor pressure.

3.2. Homogeneous nucleation model

The aerosol model combines a full kinetic treatment of the nucleation steps of the OIO

20   clusters with a "sectional" aerosol model (Raes and Janssens, 1985) to treat the growth and coagulation of the larger nucleated particles. The nucleation portion of the model consists of 20–50 bins that increment by a single OIO molecule starting with the OIO monomer. The nucleation portion of the model is coupled to a second set of bins in which the number of OIO molecules in a bin are incremented geometrically, typically by

25   a factor of 1.5. There are usually about 40 bins for the large clusters, giving a maximum particle diameter of about 1 μm.

The evolution of OIO is described by the following differential equation,

$$\frac{\partial[\text{OIO}]}{\partial t} = P - \sum_i k_i^a[\text{OIO}][i] + \sum_i k_i^d[i], \tag{9}$$

where P is the OIO production rate from the gas phase chemistry, k_i^a is the average second order rate coefficient for addition of OIO to a cluster i with concentration $[i]$, k_i^d is the average first order rate coefficient for evaporation of OIO from cluster i. OIO is produced in a series of gas phase reactions involving I atoms and ozone, that are described in the chemical mechanism section. The first sum on the right hand side of Eq. (9) accounts for the condensation of OIO, and the second sum is the rate of OIO production by cluster evaporation.

The differential equation describing the evolution of OIO cluster i is (see e.g. Raes and Janssens, 1985, 1986):

$$\frac{\partial[i]}{\partial t} = \frac{k_{i+1}^d}{n_{i+1} - n_i}[i+1]\frac{k_i^d}{n_i - n_{i-1}}[i] + \frac{k_{i-1}^a[\text{OIO}][i-1]}{n_i - n_{i-1}} - \frac{k_i^a[\text{OIO}][i]}{n_{i+1} - n_i}$$

$$+ \sum_l \sum_j k_{j,l}^c[j][l]\frac{((n_l + n_j) - n_{i-1})}{(n_i - n_{i-1})}\delta_{n_l+n_j,[n_{i-1},n_i]} + \sum_l \sum_j k_{j,l}^c[j][l]$$

$$\frac{(n_{i+1} - (n_l + n_j))}{(n_{i+1} - n_i)}\delta_{n_l+n_j,[n_i,n_{i+1}]} - \sum_j k_{i,j}^c[i][j] + \text{Wall Loss}, \tag{10}$$

where $[i]$ is the concentration of the cluster in bin i containing n_i OIO molecules, and $k_{j,l}^c$ is the average second order rate coefficient for coagulation of a cluster with n_j OIO molecules and a cluster with n_l OIO molecules. The delta function is defined by

$$\delta_{n_l+n_j,]n_{i-1},n_i]} = \begin{array}{l} 0 \text{ if } n_l + n_j \notin]n_{i-1}, n_i] \\ 1 \text{ if } n_l + n_j \in]n_{i-1}, n_i]. \end{array} \tag{11}$$

The first term on the right hand side of Eq. (11) describes the production of cluster i by the loss of OIO from the next larger cluster ($i + 1$). The second term accounts for

OIO homogeneous nucleation

J. B. Burkholder et al.

the loss of i due to evaporation of OIO. The third term is the production of i by addition of OIO to the next smaller cluster, and the fourth term is the loss of i by reaction with OIO. The fifth and sixth terms describe the production of i by coagulation of smaller clusters. The last term is the loss of cluster i by coagulation with all other clusters.

5   Coagulation coefficients are calculated by using Dahneke's (Seinfeld and Pandis, 1998, Sects. 8 and 12) form for the Brownian coagulation coefficient.

$$k_{12} = \frac{2\pi \left(D_{p1} + D_{p2}\right) \left(D_1 + D_2\right) \left(1 + Kn\right)}{1 + 2Kn(1 + Kn)/\alpha}, \tag{12}$$

where D_{pi} is the diameter of particle i, D_i is the diffusion coefficient of particle 1, Kn is the Knudsen number, and α is the accommodation coefficient. Geometric radii were

10 calculated assuming spherical clusters with variable density. The Knudsen number is given by

$$Kn = \frac{4 \left(D_1 + D_2\right)}{\overline{c_{12}} \left(D_{p1} + D_{p2}\right)}, \tag{13}$$

where $\overline{c_{12}} = \sqrt{c_1^2 + c_2^2}$ and c_i is the mean molecular speed of particle i. The diffusion constant is

$$D_i = \frac{kTC_{ci}}{3\pi\mu D_{pi}}, \tag{14}$$

15

where C_{ci} is the slip correction (Seinfeld and Pandis, 1998) and μ is the viscosity of air. OIO condensation rate coefficients were calculated with Dahneke's formula for condensation, which is the same as the coagulation equation (13) in the small cluster limit. The accommodation coefficient was set to 1.0 for OIO condensation and for

20 coagulation of all clusters with more than one OIO molecule. The set of differential equations describing cluster growth, evaporation, and coagulation was integrated by using a semi-implicit extrapolation method suitable for stiff sets of equations (Press et al., 1992).

OIO homogeneous nucleation
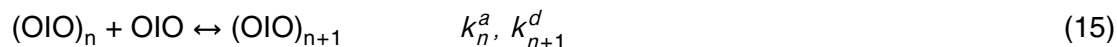
J. B. Burkholder et al.

◄◄   ►►

◄   ►

Back   Close

Full Screen / Esc

Print Version

Interactive Discussion

For the simple case of homogeneous nucleation of gas phase species OIO, the individual growth/evaporation steps are given by

$$(OIO)_n + OIO \leftrightarrow (OIO)_{n+1} \qquad k_n^a, \; k_{n+1}^d \qquad (15)$$

The growth and evaporation rate constants are related to the standard Gibbs free energy change for the reaction $(\Delta G_{n,n+1}^0)$,

$$k_p = \exp\left(\frac{-\Delta G_{n,n+1}^0}{RT}\right) = \frac{1}{RT}\frac{k_n^a}{k_{n+1}^d}, \qquad (16)$$

where K_p is the equilibrium constant with units of $1/p$ (p = standard state pressure), R is the gas constant and T is the temperature.

OIO cluster evaporation rate constants were calculated by using Dahnekes condensation rate constants and parameterized thermodynamics for the clusters. It was assumed that the OIO binding enthalpy varied as a function of the number of OIO units in the cluster as follows

$$\Delta H_{n,n+1}^0 = \Delta H_c^0 - (\Delta H_{Dimer}^0 - \Delta H_c^0)e^{-(n-1)/a}, \qquad (17)$$

where ΔH_c is the enthalpy of condensation for the bulk ($n \rightarrow \infty$), ΔH_{Dimer}^0 is the enthalpy for the OIO dimer, and a adjusts the rate of exponential variation of the enthalpy from the dimer to the bulk. The entropy change for adding OIO to all clusters was assumed to be $-0.03\,\mathrm{kcal\,mol^{-1}\,K^{-1}}$ and the Gibbs free energies were calculated as $\Delta G = \Delta H - T\Delta S$. This gives a convenient method to vary the height and position of the nucleation barrier and a "semi-physical" representation of the variation of the monomer binding energy with cluster size.

4. Results and discussion

During the course of our studies, we considered three different photolytic sources of iodine atoms (CF_3I, CH_3I, and CH_2I_2) to initiate particle production. CH_3I was used

Print Version

Interactive Discussion

in just a few preliminary measurements and found unsuitable as an iodine precursor for the reasons outlined below. First, the poor spectral overlap of the photolysis lamp output and the CH_3I absorption spectrum necessitated using relatively high initial concentrations of CH_3I (~400 ppb) to achieve the desired iodine radical production rate. When using these high concentrations, we observed significant background particle production (i.e. prior to photolysis) that was initiated by the room lights. This most likely implies that I_2 (a CH_3I impurity that photolyzes at visible wavelengths) may be responsible for the initiation of the iodine chemistry and subsequent particle production. I_2 photolysis would be a significant I atom source in the nucleation experiments, even though the BLB365 photolysis lamps do not emit strongly in the visible region, relative to that from CH_3I. The uncertainties in the iodine atom production rate associated with the I_2 impurity make CH_3I an unsatisfactory iodine precursor. Nucleation experiments were performed with both CH_2I_2 and CF_3I used as the iodine precursor. As discussed in the Experimental section, there are a number of advantages in using CF_3I as the iodine precursor. Although we have performed numerous measurements using CH_2I_2 as the iodine precursor, this data set was not used in the determination of the aerosol model parameters. However, because CH_2I_2 was used exclusively in the Hoffmann et al. (2001) and Jimenez et al. (2003) studies, some representative CH_2I_2 data, modeling, and discussion of our data are presented at the end of this section for comparison purposes.

The nucleation experimental data consists of the particle concentration as a function of time following the initiation of photolysis. In this section, we will first present some representative experimental data recorded using both continuous and pulsed photolysis. This is followed by a quantitative analysis of the data using the coupled chemical and aerosol model. For convenience of discussion, we define a parameter, τ, as the induction time between the initiation of photolysis and the initial detection of particles. Smaller values of τ indicate more efficient particle production. Other parameters that are useful in describing the efficiency of particle production are the rate of increase in particle concentration and the final particle concentration. In many cases, the final

particle concentration exceeded the upper limit of the UCPC making this diagnostic parameter of limited value. In general, the particle production temporal profiles showed good reproducibility under all the experimental variations. For example, τ was reproducible to within ~10 s while the final particle concentration was typically reproducible to within ~50%.

Examples of particle production with continuous photolysis for initial CF_3I concentrations between 5.00 and 21.0 ppb and $[O_3] = 30$ ppb are shown in Fig. 3. In these experiments τ varied from 300 to 160 s with the shortest times observed with the highest CF_3I concentration, i.e. highest radical concentrations. The particle concentration shows a rapid rise in all cases with the rate dependent on the CF_3I concentration, i.e. faster rate of rise at higher concentration. Finally, the final particle concentration observed over the first 500 s of the experiment exceeds 10^5 particle cm^{-3} for the highest CF_3I concentrations but shows a systematic decrease with decreasing CF_3I concentration for the lower values. These characteristics of the temporal profiles are evaluated quantitatively using the aerosol model.

The particle production dependence on the photolysis rate coefficient is also shown in Fig. 3. Measurements were made using the highest CF_3I concentration, 21.0 ppb, and half the photolysis lamps, i.e. half the iodine atom production rate. The particle production is nearly coincident with the particle profile recorded using full photolysis and 10.5 ppb CF_3I. This measurement along with others which are not shown using 1/2 and 1/4 of the photolysis lamps demonstrate that the particle production linearly scales with the iodine atom production rate, i.e. photolysis flux $\times[CF_3I]$. This is the expected dependence of the coupled chemical mechanism and aerosol model. The scaling with variations in photolysis flux and initial CF_3I concentration also demonstrates that the photolysis flux within the reactor is reasonably uniform in terms of particle production. For the experimental data shown in Fig. 3, the IO radical concentration rapidly rises over the first 100 s to a nearly steady-state value. The IO steady-state concentrations calculated using the chemical mechanism given in Table 2 for initial CF_3I concentrations of 5.50, 10.5, 16.1, 20.8 ppb are 10.8, 15.4, 19.5, and 22.3 ppt, respectively. The OIO

OIO homogeneous nucleation

J. B. Burkholder et al.

radical concentration increases throughout the measurement time to values of 50, 95, 102, and 104 ppt at 500 s. We should note that while the concentrations of the IO and OIO radicals in these experiments are appropriate for the evaluation of iodine oxide nucleation in the laboratory experiments they greatly exceed the concentrations measured in the atmosphere (Allan et al., 2000, 2001).

The pulsed photolysis method was used as a means to achieve lower iodine radical concentrations. An example of particle production measured using the photolysis pulse method is shown in Fig. 4. Measurements were made using 13, 22, 30, 45, 60, and 75 s of photolysis with 21.0 ppb of CF_3I and 500 ppb of O_3. This combination yields total reactive iodine concentrations of 9, 16, 21, 32, 43, and 54 ppt for the increasing durations of photolysis. As shown in Fig. 4, particle production was observed in each case although the yield was small for the 13 s photolysis measurement. The data also clearly shows a very strong non-linear dependence on the initial I atom concentration while τ varied from 600 to 150 s. For example, the final particle concentration increased nearly three orders of magnitude for a factor of three increase in the initial I atom concentration. This highly non-linear dependence is characteristic for homogeneous aerosol nucleation when a nucleation barrier exists. The particle profiles shown in Fig. 4 have some significant variations in concentration that were normally not observed in the continuous photolysis experiments. These variations may represent inhomogeneities in the particle distribution within the bag. Also shown in Fig. 4, for comparison, is the particle production measured with the same CF_3I and O_3 concentrations and continuous photolysis, τ = 140 s and 10^5 particle cm^{-3} at 210 s.

The particle formation was a function of the initial ozone concentration (with a fixed initial CF_3I or CH_2I_2 concentration and photolysis flux). An ozone dependence of the particle production was not reported in the Hoffmann et al. (2001) and Jimenez et al. (2003) studies. Particle production profiles, using continuous photolysis, with [CF_3I] = 9.80 ppb and ozone concentrations of 20, 98, and 486 ppb are shown in Fig. 5 to illustrate the O_3 dependence. In the modeling and data analysis described below, we

OIO homogeneous nucleation

J. B. Burkholder et al.

have attributed the ozone dependence to the gas phase reaction

$$IO + O_3 \rightarrow OIO + O_2 (\Delta H_r = -44 \, \text{kcal mol}^{-1}). \tag{18}$$
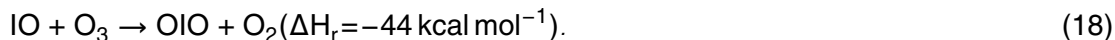
This source of OIO is pseudo-first order in IO under our experimental conditions and becomes most significant at low IO and high ozone concentrations. A global data analysis of the particle production data yielded a rate coefficient of $\sim 5 \times 10^{-15} \, \text{cm}^3$ molecule^{-1} s^{-1} for Reaction (18).

Reaction (18) has not been studied in the laboratory although rate coefficients for the analogous ClO and BrO reactions with O_3 have been reported, $< 1 \times 10^{-18} \, \text{cm}^3$ molecule^{-1} s^{-1} and $\sim 2 \times 10^{-18} \, \text{cm}^3$ molecule^{-1} s^{-1}, respectively (Sander et al., 2002), to be relatively slow. A direct rate coefficient determination for Reaction (18) would aid our assignment. It should be noted, however, that the conclusions drawn from the model analysis of the particle production data are only weakly dependent on this rate coefficient and/or its assignment in the chemical mechanism. The possible importance of Reaction (18) as an OIO source in the marine boundary layer is discussed in the Atmospheric Implications section.

4.1. Aerosol model simulations

The coupled chemical and aerosol model was used to simulate the CF_3I experimental data and determine the thermodynamic parameters, Eq. (17), that best describe the iodine oxide nucleation using the mechanism given in Table 2. The aerosol model parameters, their definitions, and their optimized values are summarized in Table 3. The optimized model simulations are shown in each of the data figures and reproduce the experimental data very well under all experimental conditions.

Although each of the model parameters are uniquely defined in the aerosol model there does exist some correlation of the model parameters in the data analysis. A sensitivity analysis for the ΔH_c, ΔH^0_{Dimer}, and a parameters was performed to evaluate the uncertainties in the individual parameters. In this analysis, the parameters were varied individually over a range of reasonable values while comparing the calculated particle

OIO homogeneous nucleation

J. B. Burkholder et al.

◄◄ | ►►

◄ | ►

Back | Close

Full Screen / Esc

Print Version

Interactive Discussion

production profiles to the experimentally measured values. From these calculations, we found that particle production was not possible for $\Delta H_c > -25$ kcal mol^{-1}. Second, provided the value of ΔH_c is below this upper limit the model results are somewhat insensitive to its value within the range -30 to -70 kcal mol^{-1}. We have taken a value

5 of -35 kcal mol^{-1} as a reasonable estimate.

The "a" parameter was varied between 2 and 7 in the sensitivity analysis. The calculations were not overly sensitive to the value of a. Reasonable fits to the experimental data were obtained with values between 3 and 5. We have taken $a = 4$ for the final analysis.

10 The modeled particle production is most sensitive to the bond enthalpy of the OIO dimer, ΔH^0_{Dimer}. In our calculations, ΔH^0_{Dimer} was varied between -14 and -22 kcal mol^{-1} with the optimum value being -17 kcal mol^{-1}. A range of ± 2 kcal mol^{-1} in ΔH^0_{Dimer} was estimated based on the range of reasonable values for the a and ΔH_c parameters. This value of ΔH^0_{Dimer} corresponds to a moderately bound OIO dimer with

15 a bond strength of ~ 17 kcal mol^{-1}. To date there are no thermodynamic parameters for the OIO dimer available in the literature with which to compare this value.

The values for the fixed parameters in the aerosol model are discussed below. Fjellvag and Kjekshus (1994) give a density of 2.57 g cm^{-3} for the I$_2$O$_4$ crystal. However, Jimenez et al. (2003) have shown that the newly nucleated iodine oxide particles are

20 fractal with a density closer to 1.0 g cm^{-3}. We have adopted this value in our aerosol model calculations as more representative of the newly formed particles. The uptake coefficient, γ, was taken to be 1.0. This is consistent with the value used in the Jimenez et al. study and represents an upper limit for the efficiency for OIO condensation. There are no direct studies of OIO uptake available in the literature. Allan et al. (2001) have

25 analyzed their OIO field measurement data using an OIO uptake coefficient of 0.02 on background aerosol in the marine boundary layer. While this value is significantly different than used in our data analysis it represents uptake on aerosol of significantly different composition than found in the laboratory studies. Direct measurement of OIO uptake coefficients on aerosol of various compositions would help to resolve this issue.

Print Version

Interactive Discussion

As shown in the experimental data figures presented so far, the aerosol model does a good job in reproducing the total particle (> 3 nm) concentration profiles. As a further test, measurements using the n-DMA with 21.0 ppb CF_3I and 30 and 300 ppb O_3 and continuous photolysis (BL350 lamps) were performed. Representative experimental data for 3, 5, 8, 10, and 15 nm diameter particles are shown in Fig. 6a. The particle concentration profiles were recorded in separate measurements under identical initial conditions. The measured profiles were independent of the initial O_3 concentration. The aerosol model calculations for these size particles are shown in Fig. 6b. The model results have been scaled to account for the n-DMA size dependent charging efficiency, as described in the operating manual, and its transfer function (Chen et al., 1998). The model profiles show good agreement with the experimental data.

4.2. Summary of CH_2I_2 experiments

Complications from background particle production, i.e. CH_2I_2/O_3 mixture but no UV photolysis, in the CH_2I_2 experiments were encountered. As observed in the CH_3I measurements, the background particle production was dependent on the room light intensity. At CH_2I_2 concentrations less than 500 ppt the background particle production was not observed over the time scale of a typical experiment, < 1000 s. Therefore, although there is an appreciable I_2 impurity it may not influence these nucleation experiments. A second complication was the general level of reproducibility in the particle production in the low CH_2I_2 concentration, < 200 ppt, experiments. The irreproducibility appeared to be dependent on the history of the reactor and are consistent with a residual CH_2I_2 concentration (of the order 10 ppt) in the reactor that was not efficiently flushed out of the bag between experiments. It should be pointed out that this was not a problem in the CF_3I experiments indicating that secondary reaction products or particle formation in the reactor was not the source of the problem. A residual CH_2I_2 concentration has the most dramatic effect on the particle production in the low concentration experiments while being insignificant in the high concentration experiments, > 200 ppt.

CH_2I_2 experiments were performed in a similar way as described above for CF_3I.

Figure 7 shows the particle production dependence on the initial CH_2I_2 concentration with ozone concentrations of 50 and 500 ppb. The background particle production in the absence of added CH_2I_2 is also shown. The background particle production was weakly dependent on the ozone concentration and is consistent with Reaction (18) leading to OIO formation. A background concentration of ~15 to 30 ppt CH_2I_2 was used to bring the model and experimental results into agreement. Similar results were observed in experiments performed using the BL350 photolysis lamps.

Photolysis pulse experiments with 185 ppt CH_2I_2, 50 ppb O_3 and photolysis times of 30, 60, 90, and 120 s are shown in Fig. 8. The photolysis durations correspond to I atom production of 6.8, 13.4, 19.7, and 25.8 ppt. The shortest photolysis duration, 30 s, did not produce a measurable particle production over the first 600 s while the aerosol model predicts a small yield. The particle production observed with the longer photolysis durations show good agreement with the model simulations and a strong non-linear dependence on the reactive iodine concentration as in the CF_3I experiments. In addition to these measurements, a single measurement at twice the initial CH_2I_2 concentration and 60 s photolysis showed reasonable agreement with the 120 s data indicating a self-consistency of the particle production with the total iodine atom production. In general, the CH_2I_2 experimental data is self-consistent with the CF_3I data provided a small CH_2I_2 background concentration is included in the model calculations.

4.3. Particle production temperature dependence

The experimental data presented so far was recorded at 298 K. The chemical reaction mechanism (and therefore the iodine radical concentrations) is relatively insensitive to small changes in temperature. However, cluster formation and particle nucleation are expected to demonstrate a strong temperature dependence mostly due to the strong temperature dependence of cluster evaporation. The temperature dependence could play an important role in particle formation in the colder regions of the atmosphere. Therefore, we have evaluated the particle production temperature dependence in ex-

OIO homogeneous nucleation

J. B. Burkholder et al.

Title Page

Abstract	Introduction
Conclusions	References
Tables	Figures

◀◀   ▶▶

◀   ▶

Back   Close

Full Screen / Esc

Print Version

Interactive Discussion

periments performed at two different initial CF$_3$I concentrations (21.0 and 5 ppb) at 296, 308, and 318 K. The experimental data is summarized in Fig. 9. At 21.0 ppb CF$_3$I, τ did not change with temperature within the precision of the measurement. However, the rate of increase in the particle concentration decreased with increasing temperature. At 5.5 ppb CF$_3$I, τ was observed to increase with increasing temperature.

Aerosol model simulations using the parameters determined from the analysis of the CF$_3$I room temperature data are also shown in Fig. 9. In general, the model simulations qualitatively reproduce the effects of temperature but do not capture the dependence on temperature quantitatively. These measurements show that temperature will have a significant influence on the efficiency of particle production in the iodine oxide system. Further work is needed to refine the potentially important effect of temperature on particle production.

4.4. Comparison with previous studies

Aerosol formation has been observed in iodine/ozone reaction systems and reported in numerous studies (Cox and Coker, 1983; Harwood et al., 1997; Hoffmann et al., 2001; Jimenez et al., 2002). The more recent studies of Hoffmann et al. (2001) and Jimenez et al. (2003) provide the most quantitative data for comparison with the present work and are considered in more detail here. In both studies, UV photolysis of CH$_2$I$_2$ in the presence of excess O$_3$ was used to initiate gas phase iodine chemistry (see reaction mechanism above and Table 2 in Jimenez et al. (2003) for details) leading to new particle formation. Hoffmann et al. used relatively high initial concentrations of CH$_2$I$_2$ (4 and 17 ppb) while Jimenez et al. made measurements at lower, more atmosphericly relevant, CH$_2$I$_2$ concentrations (down to 15 ppt). Based on their mass spectrometric aerosol composition measurements and previously published studies of iodine oxides, Hoffmann et al. proposed that OIO was responsible for the observed particle formation. However, particle formation under these highly super-saturated conditions (i.e. high radical concentrations) is insensitive to the thermodynamics of the initial nucleation steps (i.e. nucleation is near the collision limit). Therefore, a quantitative comparison

OIO homogeneous nucleation

J. B. Burkholder et al.

Title Page

Abstract	Introduction
Conclusions	References
Tables	Figures

◄ ►│

◄ ►

Back Close

Full Screen / Esc

Print Version

Interactive Discussion

© EGU 2003

using our aerosol model with the Hoffmann et al. data was not pursued.

Jimenez et al. (2003) have reported data for iodine oxide aerosol formation under a wider range of experimental conditions (initial CH_2I_2, relative humidity, and CH_2I_2 photolysis rate coefficients) than used in the Hoffmann et al. study. Their measurements made with lower CH_2I_2 concentrations, < 5 ppb, provide data which is more sensitive to the initial iodine oxide nucleation steps and therefore are appropriate for comparison within the framework of our aerosol model. The experiments of Jimenez et al. also provided quantitative information for the physical properties of the iodine aerosol (density, hygroscopicity) and composition that were incorporated into the development of our aerosol model.

A comparison of aerosol model simulations (or our experimental data) with the data reported by Jimenez et al. has caveats. In principle, the experiments are similar in design and a direct comparison of results could be made. However, there are differences in the experimental particle sampling methods used that impede a direct comparison. Jimenez et al. extended the concentration range of their particle counter by diluting the aerosol sampling flow by a factor of 1000, yielding an upper limit of 10^8 particle cm^{-3} for the UCPC. The dilution was necessary in their experiments to enable monitoring of the particle growth following the initial nucleation burst. Our measurements did not employ a sample dilution and were therefore limited to particle concentrations less than 10^5 particle cm^{-3}. Diluting the sample has several effects that result in decreased particle detection efficiency. The decreased efficiency is greatest for small particles and was estimated by Jimenez et al. to be $\sim$0.17%, 8.4%, 30%, and 88% for 3, 6, 10, and 50 nm diameter particles, respectively. Uncertainties in the detection efficiency are a primary limitation in the comparison of the Jimenez et al. experimental data and our aerosol model calculations.

We have used the values of τ and the peak particle concentration reported by Jimenez et al. (2003) to compare with our aerosol model simulations. We found the modeled values of τ to be systematically greater, $\sim$10%, than the reported values. Direct experimental measurements of the particle detection efficiency in the Jimenez

OIO homogeneous nucleation

J. B. Burkholder et al.

et al. measurements as a function of particle size would be necessary to refine this analysis. Jimenez et al. show the particle concentration profile for their 5 ppb CH_2I_2 base-case measurements. For these conditions the modeled rate of rise in the particle concentration was more rapid than observed. This rate is, however, sensitive to the photolysis rate coefficient and a small decrease, ~25%, in this value is sufficient to re-produce the experimentally observed rate of rise in the particle concentration. Finally, the peak particle concentrations calculated in our aerosol model are systematically higher, approximately a factor of four, than the reported values. Considering all the assumptions made in this analysis, we consider this to be reasonable agreement.

We should also point out that the model evaluation of the Jimenez et al. 15 ppt CH_2I_2 data is extremely sensitive to the initial concentration. An uncertainty in the initial CH_2I_2 concentration of a few ppt has a dramatic affect on both τ and the final particle concentration. The experimental data was reproduced in our model using an initial CH_2I_2 concentration of 18 ppt. In conclusion, this semi-quantitative model analysis of the Jimenez et al. data demonstrates a reasonable level of consistency with the results of our nucleation experiments.

5. Atmospheric implications

In this section, we address the significance of the iodine oxide aerosol production on both local and regional scale in the marine boundary layer (MBL). We have used the recently reported field measurements of IO, OIO, and ultra-fine aerosol and the aerosol model parameters determined in this study in a box-model to evaluate the efficiency of the iodine oxide aerosol formation in the MBL. We present results from three model calculations in which OIO is assumed to be the homogeneous nucleating species with the mechanism outlined in this paper. Two calculations utilize the field observations of OIO and IO to define their concentrations. The final calculation evaluates the possible influence of localized "hot" spots in the iodine oxide concentrations on the aerosol production. In this calculation, we have extended the calculations beyond the range of

the field measurements to evaluate under what atmospheric concentrations of IO and OIO aerosol formation can be expected.

In the first atmospheric box-model calculation we address the question: *What concentration of OIO is required to yield the particle concentrations observed at Mace Head station?* Field measurements of OIO are very limited. In fact, Allan et al. (2001) have reported the only field measurement of OIO off the coast of Cape Grim, Tasmania. The OIO concentration was below the detection limit, ~0.5 ppt, during daylight and increased to ~3 ppt for several hours just after sunset. Measurements of aerosol production were not reported as part of this study. Measurements of the OIO concentration at the Mace Head station during the period of the PARFORCE have not been reported in the literature. In our model, the particle concentration as a function of time was calculated as a function of a steady-state OIO concentration. The model was run for two hours to cover the time frame for aerosol formation observed during the PARFORCE campaign at Mace Head station. Calculations were performed using the optimized model parameters (determined above) with OIO steady state concentrations between 0.5 and 100 ppt at temperatures of 270, 280, 290, and 300 K. The model results are summarized in Fig. 10.

It is evident from Fig. 10 that OIO steady-state concentrations similar to the value reported by Allan et al. (2001), ~0.5 ppt, are not sufficient to yield the particle concentrations observed at Mace Head station. In fact, an OIO concentration of 0.5 ppt would not yield measurable particle formation within 2 h. However, a steady-state concentration of 10 ppt would yield 10^6 particle cm^{-3} within 10 to 20 min and be more consistent with the particle production observed at Mace Head Atmospheric Research station. It may be possible that high concentrations of OIO, > 10 ppt, are present in localized "hot" spots along the coast region. In this case the coast region would consist of an inhomogeneous source of OIO. Following dilution of the aerosol produced in the "hot" spot, this could still account for the observed particle concentrations. More extensive and localized field measurements of OIO in the MBL and its correlation with aerosol production would be invaluable in evaluating this hypothesis. Although the particle pro-

duction dependence on temperature was not accurately defined in the present study, the atmospheric box-model calculations shown in Fig. 10 demonstrate its importance. For example, a factor of 1000 increase in particle yield is calculated for a decrease in temperature from 300 K to 270 K.

5   The flux of iodine containing compounds in the open ocean is expected to differ significantly from that found in the coastal regions. In the coastal regions, emission of CH_2I_2 from macroalgae under stress (i.e. low tide) is expected to be much larger than found in the open ocean. The lone field measurement of OIO, < 0.5 ppt, at Cape Grim, Tasmania may therefore be more representative of the open ocean conditions.

10 Our aerosol model calculations would lead us to conclude that OIO homogeneous nucleation in the open ocean would not be a significant source of MBL aerosol.

    In the second model calculation, an approach that relies on the extensive field observations of the IO radical was used. There are a number of high quality field measurements of IO in the MBL made using long path absorption techniques (Alicke et

15 al., 1999; Allan et al., 2000, 2001; Frieb et al., 2001). These measurements provide an important guide to iodine oxide aerosol formation because IO is the precursor for OIO formation either through Reaction (3), IO + IO, or via IO + BrO (Rowley et al., 2001). The IO + BrO reaction is expected to be a minor source of OIO in the MBL due to the low BrO concentrations. Under certain conditions common to the open ocean,

20 Reaction (18), IO + O_3, could be the major source of OIO.

    The measured IO concentration shows a strong correlation with solar flux and reaches values up to ~6 ppt at mid-day and below the detection limit (0.5 ppt) at night. The peak IO concentrations measured in three separate locations (Mace Head, Ireland; Tenerife, Canary Islands; and Cape Grim, Tasmania) by Allan et al. (2001) were

25 very similar, ~2 ppt. Alicke et al. (1999) report slightly higher values in their measurements at Mace Head, Ireland. The differences in the two Mace Head, Ireland studies may reflect differences in the air masses sampled. For example, much of the optical path length (8.4 km) in the Allan et al. study (EASE 97) was over the open sea between Croaghnakeela Island and the Mace Head station. Therefore fluctuations in the

OIO homogeneous nucleation

J. B. Burkholder et al.

Print Version

Interactive Discussion

IO concentrations in the coastal region may have been poorly sampled.

Using known gas phase chemistry of the IO radical, the OIO concentration and the resulting particle production was modeled. In this calculation the atmospheric loss processes for OIO such as reaction, deposition, and photolysis that are currently not very well characterized need to be included. Reaction of OIO with Cl, OH and NO are the most likely reactive losses for OIO in the MBL. Rate coefficients for these reactions on the order of 10^{-12} cm^3 molecule^{-1} s^{-1} for OH and NO and 10^{-10} cm^3 molecule^{-1} s^{-1} for Cl reactions are reasonable estimates. Only the NO concentration is expected to be high enough in the MBL, 10 to 20 ppt, to possibly have an impact on iodine oxide aerosol formation. Uptake of OIO on background aerosol would also limit the OIO concentration. The uptake loss rate will depend on the background aerosol concentration and the efficiency of OIO uptake. In their field measurements, Allan et al. (2001) attributed loss of OIO after sunset to uptake on background aerosol with a lifetime of several hours. Photodissociation of OIO in its visible absorption band

$$OIO + h\nu \rightarrow O + IO \tag{19a}$$

$$\rightarrow I + O_2 \tag{19b}$$

is potentially the most significant loss process for OIO in the MBL. OIO photolysis lifetimes on the order of seconds are possible provided that absorption over the entire visible absorption band leads to photodissociation. The threshold for Reaction (19a) has been calculated to be at $\sim$410 nm (Misra and Marshall, 1998) while Reaction (19b) is possible over the entire absorption band. Either channel would directly affect the efficiency of aerosol production through the loss of OIO.

The box-model was run over a 12 h period using a diurnal cycle for the IO concentration as reported by Allan et al. (2000). Calculations were performed with peak IO concentration values of 0.5, 1.0, 3.0, and 5.0 ppt to cover the range observed in the field measurements. The OIO first order loss rate coefficient, k_{19}, was varied over the range 0 to 0.05 s^{-1} in these calculations. The peak particle concentration and maxi-

⏮ | ⏭

◀ | ▶

Back | Close

Full Screen / Esc

Print Version

Interactive Discussion

mum OIO concentration, $[OIO]_{max}$, reached during the 12 h period for these conditions are summarized in Fig. 11.

The first conclusion drawn from this calculation is that significant aerosol production occurs within the first few hours for each of the IO concentrations used provided $k_{19} <$ 0.005 s^{-1}. The OIO concentration reaches values of 10's of ppt near the end of the calculation for $k_{19} < 0.005$ s^{-1}. Second, particle production and the $[OIO]_{max}$ values have a very strong dependence on the value of k_{19}, i.e. they rapidly decrease with increasing k_{19}. An accurate value of k_{19} is crucial to the evaluation of this aerosol production mechanism. These calculations also demonstrate that OIO loss processes such as reaction and uptake that are on the order of 10^{-4} s^{-1} may only be minor relative to the photolysis loss.

In the third model calculation we address the question: *What IO concentration would be needed to achieve the observed aerosol production at Mace Head station?* As demonstrated in the calculations presented above, the OIO steady state concentration needs to be in the 10 ppt range to yield the observed particle concentrations. To a first approximation, $[OIO]_{ss}=k_3[IO]_{ss}^2/k_{19}$ which implies, depending on the value of k_{19}, that $[IO]_{ss}$ would need to be in the range of 10 s to 100 s ppt. The box-model calculation results for a range of $[IO]_{ss}$ values from 50 to 200 ppt and k_{19} values from 0.25 to 2 s^{-1} are shown in Fig. 12. The value of $k_{19} = 2$ s^{-1} represents a reasonable upper limit for the photolysis rate coefficient of OIO in the MBL. This calculation shows that the observed particle concentrations at Mace Head (and their rapid formation) can be reproduced with $[IO]_{ss}$ of 50 to 100 ppt. These high IO concentrations are in conflict with the published field measurements of IO (derived from long path absorption measurements) but would be consistent with the hypothesis of localized "hot" spots of high iodine emission.

6. Conclusions

In this work, iodine oxide nucleation was examined using laboratory measurements of new particle production and analysis with a coupled chemical-aerosol model. It is observed that new particle formation in this system is efficient. Model parameters that describe the single component homogeneous nucleation of OIO are determined. Atmospheric box-model calculations show that the IO and OIO concentrations reported in the recent field measurements in the marine boundary layer (Allan et al., 2000, 2001) are not sufficient to account for significant aerosol production either in the coastal or open ocean marine boundary layer. Model calculations demonstrate that inhomogeneous sources of iodine oxides, i.e. "hot" spots with elevated iodine precursor (i.e. CH_2I_2) emissions, could possibly account for the observed large aerosol production in the coastal region at Mace Head station. This hypothesis awaits confirmation by future field and laboratory studies.

References

Allan, B. J., McFiggans, G., Plane, J. M. C., and Coe, H.: Observations of iodine monoxide in the remote marine boundary layer, J. Geophys. Res., 105, 14 363–14 369, 2000.

Allan, B. J., Plane, J. M. C., and McFiggans, G.: Observations of OIO in the remote marine boundary layer, Geophys. Res. Lett., 28, 1945–1948, 2001.

Alicke, B., Hebestreit, K., Stutz, J., and Platt, U.: Iodine oxide in the marine boundary layer, Nature, 397, 572–573, 1999.

Ashworth, S. H., Allan, B. J., and Plane, J. M. C.: High resolution spectroscopy of the OIO radical: Implications for the ozone-depleting potential of iodine, Geophys. Res. Lett., 29, doi: 10.1029/2001GL013851, 2002.

◀◀ | ▶▶

◀ | ▶

Back | Close

Full Screen / Esc

Print Version

Interactive Discussion

Bloss, W. J., Rowley, D. M., Cox, R. A., and Jones, R. L.: Kinetics and products of the IO self-reaction, J. Phys. Chem. A, 105, 7840–7854, doi: 10.1021/jp012429y, 2001.

Carpenter, L. J., Hebestreit, K., Platt, U., and Liss, P. S.: Coastal zone production of IO precursors: a 2-dimensional study, Atmos. Chem. Phys., 1, 9–18, 2001.

Chen, D.-R., Pui, D. Y. H., Hummes, D., Fissan, H., Quant, F. R., and Sem, G. J.: Design and evaluation of a nanometer aerosol differential mobility analyzer (nano-DMA), J. Aerosol Science, 29, 497–509, 1998.

Cox, R. A. and Coker, G. B.: Absorption cross section and kinetics of IO in the photolysis of CH_3I in the presence of ozone, J. Phys. Chem., 87, 4478–4484, 1983.

Fjellvag, H. and Kjekshus, A.: The crystal structure of I_2O_4 and its relations to other iodine-oxygen-containing compounds, Acta Chemica Scandinavica, 48, 815–822, 1994.

Frieb, U., Wagner, T., Pundt, I., Pfeilsticker, K., and Platt, U.: Spectroscopic measurements of tropospheric iodine oxide at Neumayer Station, Antarctica, Geophys. Res. Lett., 28, 1941–1944, 2001.

Harwood, M. H., Burkholder, J. B., Hunter, M., Fox, R. W., and Ravishankara, A. R.: Absorption cross sections and self-reaction kinetics of the IO radical, J. Phys. Chem. A, 101, 853–863, 1997.

Hoffmann, T., O'Dowd, C. D., and Seinfeld, J. H.: Iodine oxide homogeneous nucleation: An explanation for coastal new particle production, Geophys. Res. Lett., 28, 1949–1952, 2001.

Ingham, T., Cameron, M., and Crowley, J. N.: Photodissociation of IO (355 nm) and OIO (532 nm): Quantum yields for $O(^3P)$ and $I(^2PJ)$ production, J. Phys. Chem. A., 104, 8001–8010, 2000.

Jimenez, J. J., Cocker, D. R., Bahreini, R., Zhuang, H., Varutbangkul, V., Flagan, R. C., and Seinfeld, J. H.: New particle formation from photooxidation of diiodomethane (CH_2I_2), J. Geophys. Res., 108, D10, 4318, doi: 10.1029/2002JD002452, 2003.

Kavouras, I. G., Mihalopoulos, N., and Stephanou, E. G.: Formation of atmospheric particles from organic acids produced by forests, Nature, 395, 683–686, 1998.

Kavouras, I. G., Mihalopoulos, N., and Stephanou, E. G.: Formation and gas/particle partitioning of monoterpenes photo-oxidation products over forests, Geophys. Res. Lett., 26, 55–58, 1999.

Leaitch, W. R., Bottenheim, J. W., Biesenthal, T. A., Li, S. M., Liu, S. K., Asalien, K., Dryfhout-Clark, H., Hopper, F., and Brechtel, F.: A case study of gas-to-particle conversion in an eastern Canadian forest, J. Geophys. Res., 104, 8095–8111, 1999.

OIO homogeneous nucleation

J. B. Burkholder et al.

Title Page

Abstract	Introduction
Conclusions	References
Tables	Figures

◀◀ ▶▶

◀ ▶

Back Close

Full Screen / Esc

Print Version

Interactive Discussion

Marti, J. J., Weber, R. J., McMurry, P. H., Eisele, F. L., Tanner, D. J., and Jefferson, A.: New particle formation at a remote continental site: Assessing the contribution of SO_2 and organic precursors, J. Geophys. Res., 102, 6331–6339, 1997.

Misra, A. and Marshall, P.: Computational investigations of iodine oxides, J. Phys. Chem. A, 102, 9056–9060, 1998.

O'Dowd, C. D., Hämeri, K, Mäkelä, J. M. et al.: A dedicated study of new particle formation and fate in the coastal environment (PARFORCE): Overview of objectives and achievements, J. Geophys. Res. 107, D19, 8108, doi:10.1029/2001JD000555, 2002.

Press, W. H., Teukolsky, S. A., Wetterling, W. T., Flannery, B. T.: Numerical Recipes in Fortran 77: the Art of Scientific Computing, Cambridge University Press, Cambridge 1992.

Raes, F. and Janssens, A.: Ion-induced aerosol formation in a $H_2O-H_2SO_4$ system – I. Extension of the classical theory and search for experimental evidence, J. Aerosol Sci. 16, 217–227, 1985.

Raes, F. and Janssens, A.: Ion-induced aerosol formation in a $H_2O-H_2SO_4$ system – II. Numerical calculations and conclusions, J. Aerosol Sci. 17, 715–722, 1986.

Roehl, C. M., Burkholder, J. B., Moortgat, G. K., Ravishankara, A. R., and Crutzen, P. J.: Temperature dependence of UV absorption cross sections and atmospheric implications of several alkyl iodides, J. Geophys. Res. 102, D11, 12 819–12 829, 1997.

Rowley, D. M., Bloss, W. J., Cox, R. A., and Jones, R. L.: Kinetics and products of the IO + BrO reaction, J. Phys. Chem. A, 105, 7855–7864, doi: 10.1021/jp004494y, 2001.

Sander, S. P., Finlayson-Pitts, B. J., Friedl, R. R., Golden, D. M., Huie, R. E., Kolb, C. E., Kurylo, Molina, M. J., Moortgat, G. K., Orkin, V. L., and Ravishankara, A. R.: Chemical kinetics and photochemical data for use in atmospheric studies, Evaluation 14, JPL publ. 02-25, http://jpldataeval.jpl.nasa.gov/, 2002.

Seinfeld, J. H. and Pandis, S. N.: Atmospheric Chemistry and Physics, John Wiley & Sons, New York 1998.

Solomon, S., Burkholder, J. B., Ravishankara, A. R., and Garcia, R. R.: Ozone depletion and global warming potentials of CF_3I, J. Geophys. Res., 99, D10), 20 929–20 935, 1994.

Turnipseed, A. A., Gilles, M. K., Burkholder, J. B., and Ravishankara, A. R.: LIF detection of IO and the rate coefficients for I + O_3 and IO + NO reactions, Chem. Phys. Lett., 242, 427–434, 1995.

OIO homogeneous nucleation

J. B. Burkholder et al.

Table 1. Photolysis rate coefficients[a]

Molecule	BL350 Lamp (s^{-1})	BLB365 Lamp (s^{-1})
CH_2I_2	1.7×10^{-2}	1.25×10^{-3}
CF_3I	3.3×10^{-5}	3.0×10^{-6}
O_3	9.5×10^{-5}	8.2×10^{-6}
IO	0.18	0.15
OIO^{b}	7.5×10^{-4}	7.5×10^{-4}
I_2	6.5×10^{-4}	1.8×10^{-4}

[a] Reported photolysis rate coefficients are with 24 lamps in the geometry described in the text.
[b] The photolysis rate coefficients for OIO were calculated using an absorption spectrum normalized to a cross section of 1.1×10^{-17} cm^2 molecule^{-1} at the peak near 540 nm. The OIO quantum yield was assumed to be unity.

Table 2. Gas phase reaction mechanism

Reaction		#	Rate coefficient cm^3 molecule^{-1} s^{-1}	Reference
$CH_2I_2 + h\nu$	$\rightarrow$ Products + I	1	See Table 1	
$CF_3I + h\nu$	$\rightarrow$ Products + I	1	See Table 1	
$I + O_3$	$\rightarrow$ IO + O_2	2	1.2×10^{-12}	Turnipseed et al. (1995)
IO + IO	$\rightarrow$ Products	3(a–e)	1×10^{-10}	Harwood et al. (1997)
	$\rightarrow$ 2I + O_2	3(a)		
	$\rightarrow$ $I_2 + O_2$	3(b)	$\Phi = 0.05$	
	$\rightarrow$ OIO + I	3(c)	$\Phi = 0.30$	Bloss et al. (2001)
	$\rightarrow$ IOI + O	3(d)		
	$\rightarrow$ I_2O_2	3(e)		
$IO + O_3$	$\rightarrow$ OIO + O_2	18	$\sim 5 \times 10^{-15}$	This work

Title Page

Abstract | Introduction

Conclusions | References

Tables | Figures

◄◄ | ►►

◄ | ►

Back | Close

Full Screen / Esc

Print Version

Interactive Discussion

Table 3. Aerosol model parameter definitions and optimized values

Parameter	Definition	Value
Variable		
ΔH_c	Enthalpy of OIO Condensation	-35 kcal mol^{-1}
ΔH_{Dimer}^0	Bond Enthalpy of OIO Dimer	-17 kcal mol^{-1}
a	Transition: Dimer to Bulk	4
Fixed		
ρ	Density of OIO cluster	1.0 g cm^{-3}
γ	OIO Uptake Coefficient	1.0
r	UCPC: Particle radius detection limit	1.5 nm
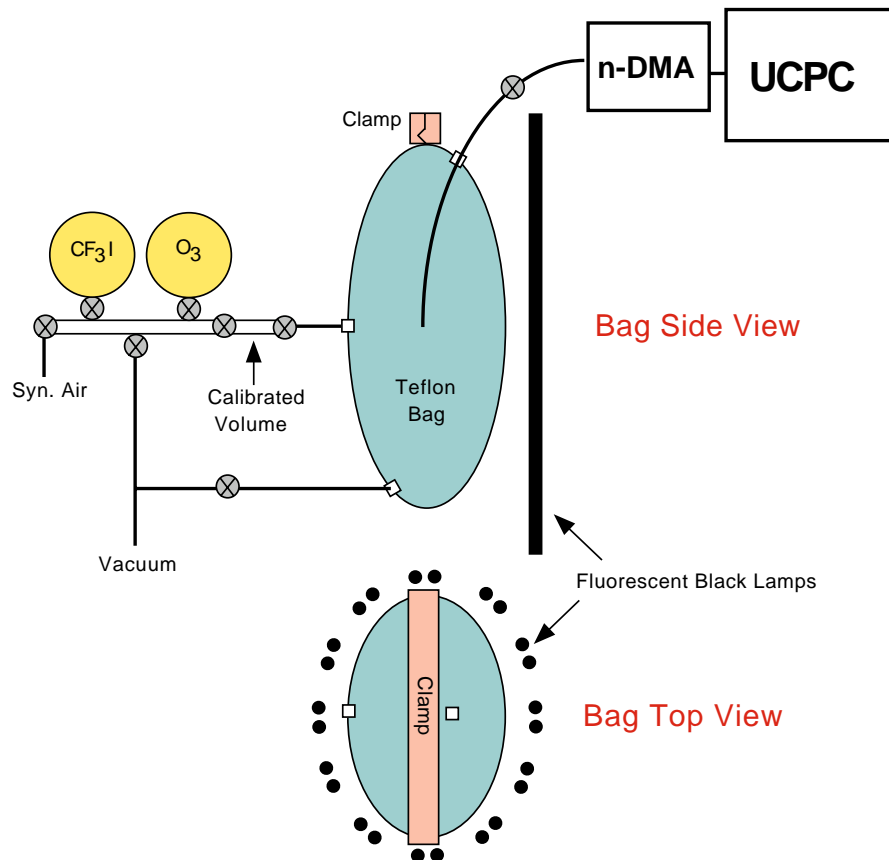
Fig. 1. Diagram of experimental apparatus. Fluorescent black lamps: BL350 or BLB365; n-DMA = nano-Differential Mobility Analyzer; UCPC = Ultra-fine Condensation Particle Counter.
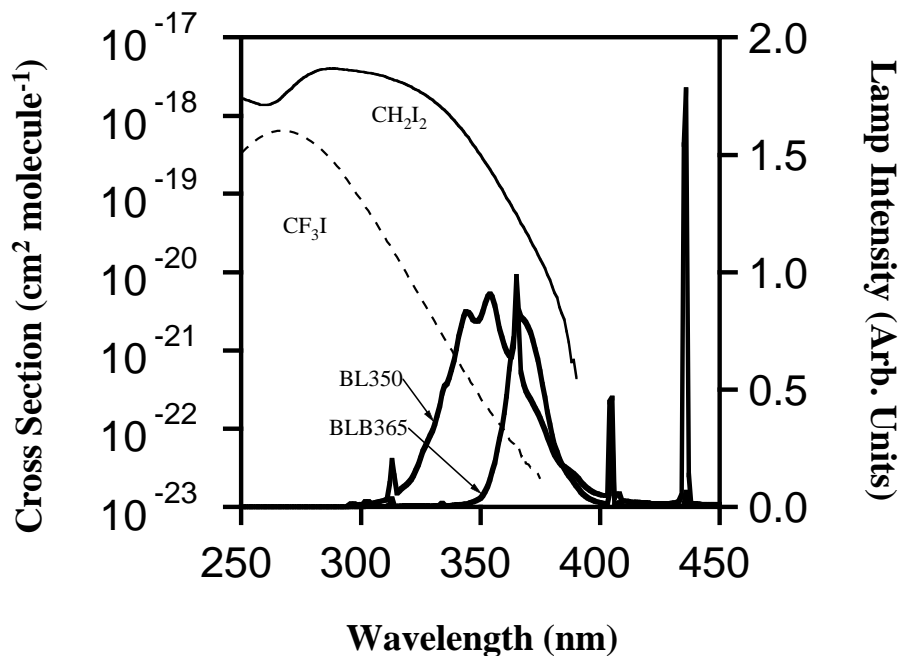
Fig. 2. Comparison of the BL350 and BLB365 photolysis lamp spectra with the absorption spectra of the CF_3I and CH_2I_2 precursors used in the nucleation experiments.

Title Page

Abstract | Introduction

Conclusions | References

Tables | Figures

|◄ | ►|

◄ | ►

Back | Close

Full Screen / Esc

Print Version

Interactive Discussion
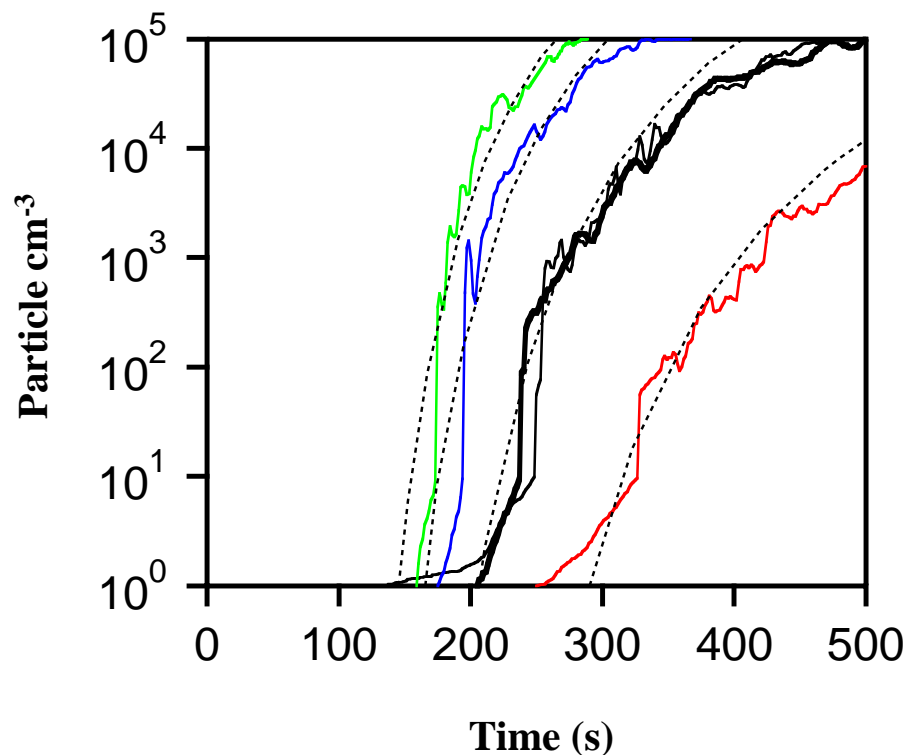
Fig. 3. Dependence of particle production on the initial CF_3I concentration with a fixed ozone concentration, 30 ppb, and BL350 photolysis lamps (24 total). The CF_3I concentrations were: 5.50 (red), 10.5 (black), 16.1 (blue), 20.8 (green) ppb (solid lines, right to left). BL350 photolysis lamps (24 total) were used. The scaling of the particle production with the photolysis flux and initial CF_3I concentration is illustrated for half the photolysis flux (12 lamps) and 21.0 ppb CF_3I (heavy black line). The aerosol model simulations are shown as dashed line (see text for details).
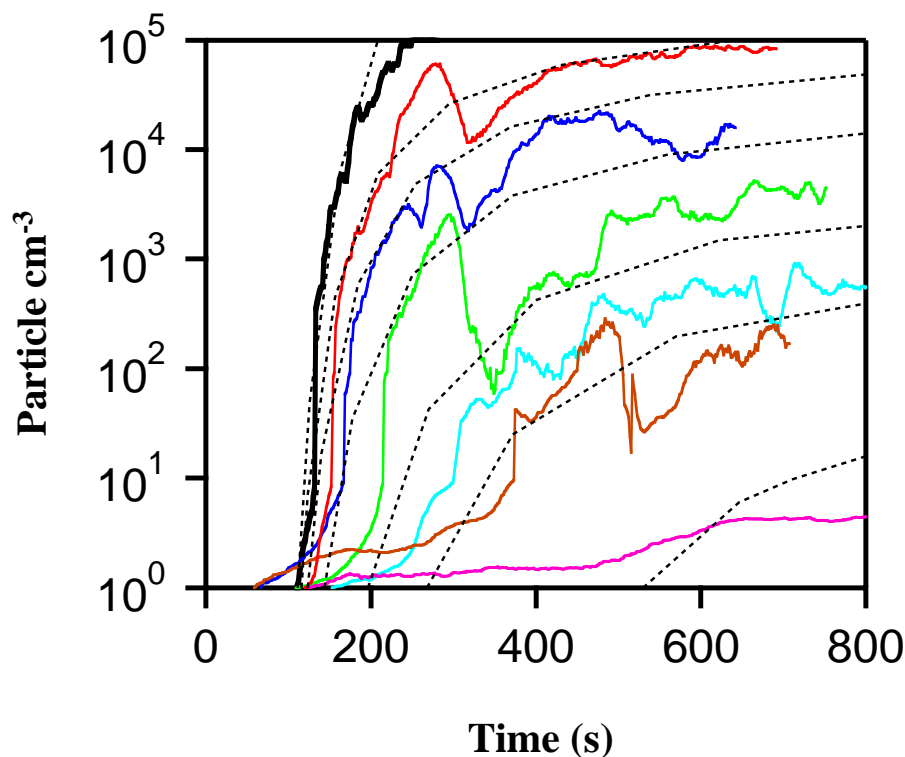
Fig. 4. Particle production following 13 s (purple), 22 s (brown), 30 s (light blue), 45 s (green), 60 s (blue), and 75 s (red) pulses of photolysis with 21.0 ppb CF_3I and 500 ppb O_3. The particle profile obtained with continuous photolysis is shown as the heavy black line. The aerosol model simulations are shown as dashed lines.
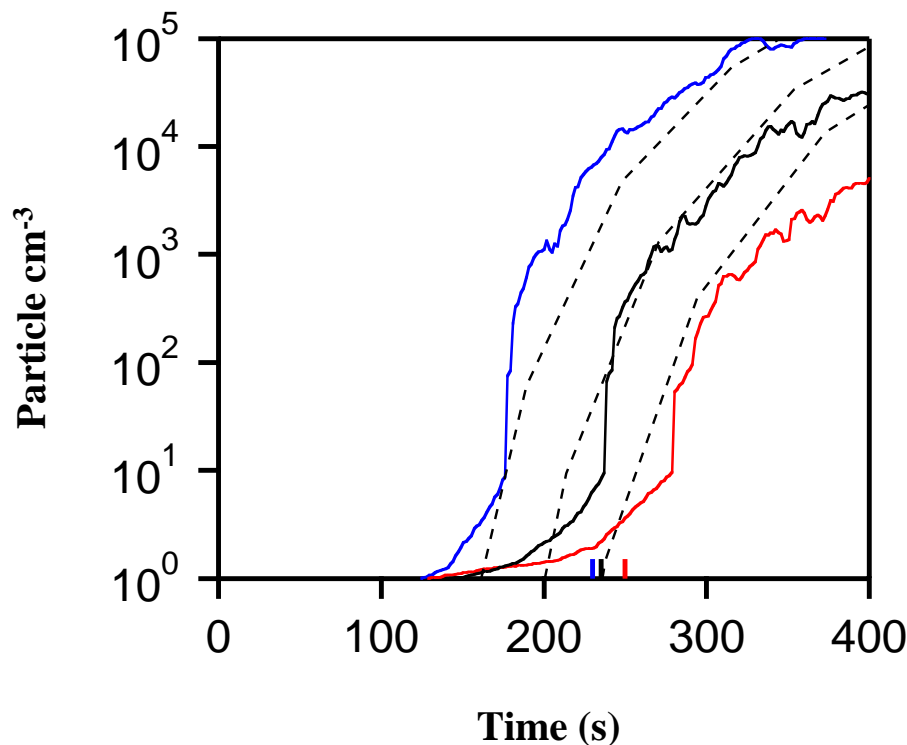
Fig. 5. Ozone dependence of the iodine oxide particle formation. Ozone concentrations are 20 (red), 98 (black), and 486 (blue) ppb with a fixed initial CF_3I concentration of 9.80 ppb. Aerosol model calculations (dashed lines) were made with k_{18}($IO + O_3 \rightarrow OIO + O_2$=5 × 10^{-15} cm^3 molecule^{-1} s^{-1}. The vertical lines on the time axis indicate the aerosol model calculated values of τ without the $IO + O_3$ reaction included in the model (lowest ozone concentration on the right).

Title Page

Abstract | Introduction

Conclusions | References

Tables | Figures

◄◄ | ►►

◄ | ►

Back | Close

Full Screen / Esc

Print Version

Interactive Discussion

OIO homogeneous nucleation

J. B. Burkholder et al.
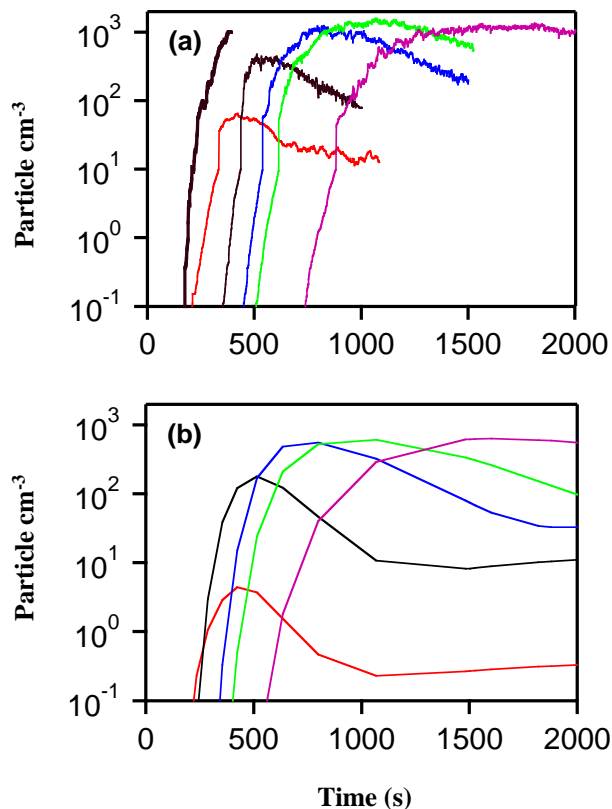
Fig. 6. Particle concentration profiles measured using the n-DMA with BL350 photolysis lamps (24) and 21.0 ppb CF_3I and 30 ppb O_3. **(a)** Measured concentrations: 3 nm (red), 5 nm (black), 8 nm (blue), 10 nm (green), and 15 nm (purple) diameter particles. The measured total particle concentration (> 3 nm dia.) under these conditions divided by 100 is given at the far left. **(b)** The corresponding particle size profiles calculated using the aerosol model and parameters determined in this work.

Fig. 7. Particle production dependence on the initial CH_2I_2 concentration measured using BLB365 lamp continuous photolysis. **(a)** initial CH_2I_2 concentrations of 0 (red), 15 (black), 29 (blue), 45 (green), 93 (purple), 531 (brown), and 1500 (light blue) ppt with 50 ppb O_3. **(b)** initial CH_2I_2 concentrations were 0 (red, two measurements), 6.6 (black), 13.7 (blue), 26.1 (green), and 41.4 (purple) ppt with 500 ppb O_3. The aerosol model simulations are shown as dashed lines (see text for details).
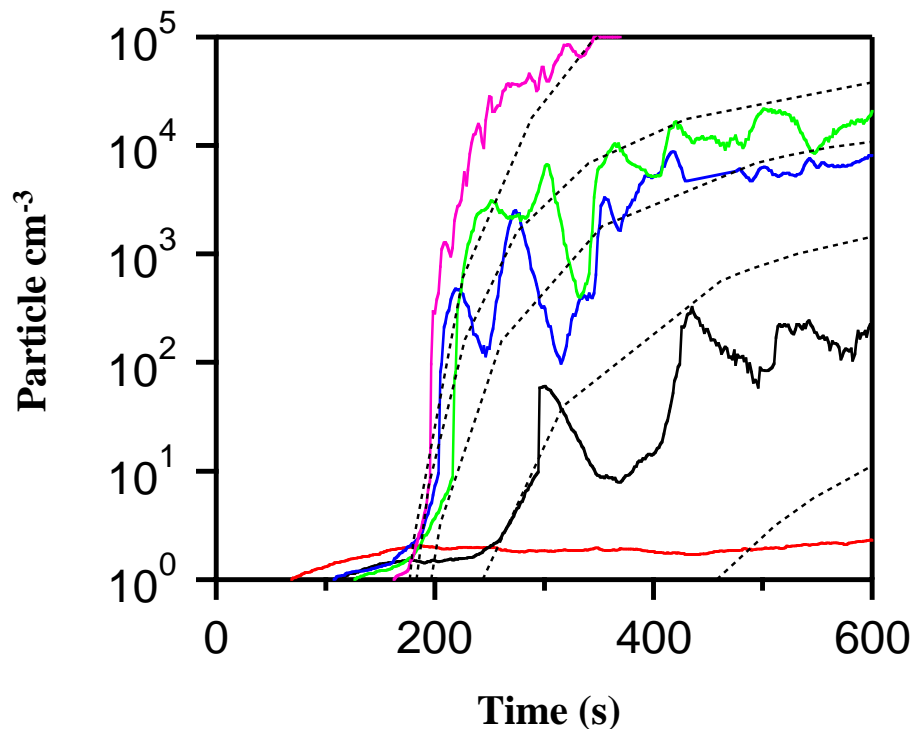
Fig. 8. Particle production following 30 s (red), 60 s (black), 90 s (blue), and 120 s (green) photolysis pulses (BLB365 lamps) with 185 ppt CH_2I_2 and 50 ppb O_3. The particle production measured under these concentrations with continuous photolysis is shown for comparison (purple). The photolysis pulses correspond to I atom production concentrations of 6.8, 13.4, 19.7, and 25.8 ppt, respectively. The aerosol model simulations are given as the dashed lines (see text for details).

Title Page

Abstract | Introduction

Conclusions | References

Tables | Figures

◄◄ | ►►

◄ | ►

Back | Close

Full Screen / Esc

Print Version

Interactive Discussion

Fig. 9. Particle production temperature dependence measurements. Experimental data **(a)** measured with [CF$_3$I] = 21.0 ppb at 296 K (red) and 318 K (green) **(b)** with [CF$_3$I] = 5.5 ppb at 296 K (red), 308 K (green), and 318 K (blue). The aerosol model simulations are shown as the short dashed lines (see text for details).

Title Page

Abstract | Introduction

Conclusions | References

Tables | Figures

◄◄ | ►►

◄ | ►

Back | Close

Full Screen / Esc
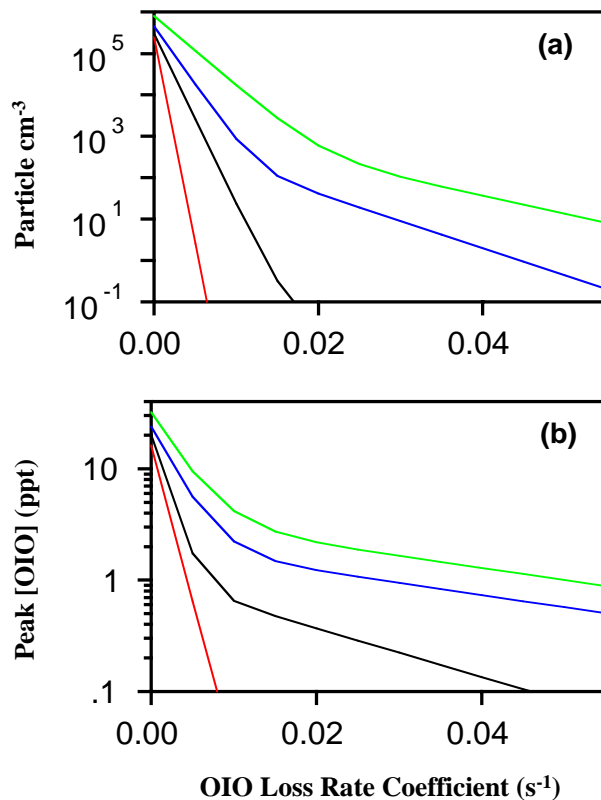
Print Version

Interactive Discussion

© EGU 2003
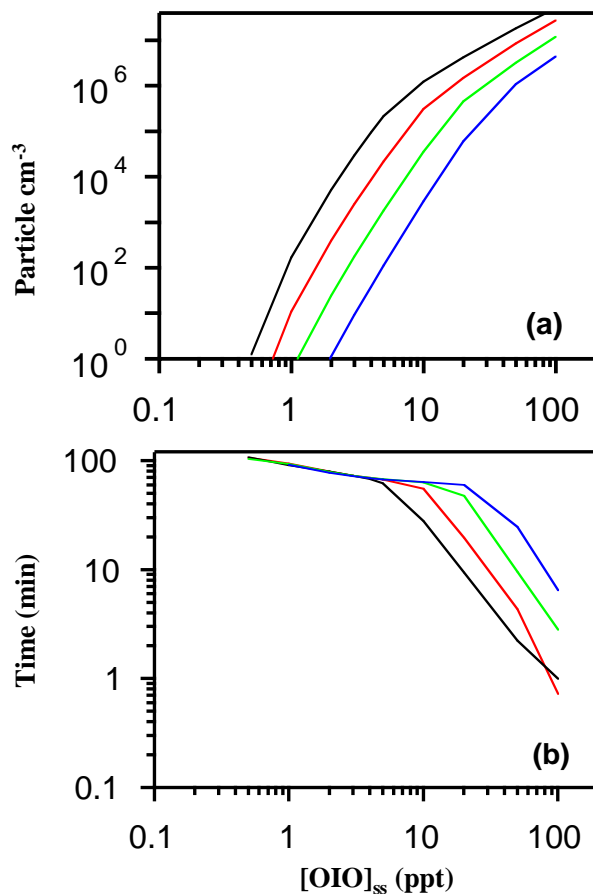
Fig. 10. Aerosol production ($d > 3$ nm) calculated assuming a steady state concentration of OIO at 270 K (black), 280 K (red), 290 K (green), and 300 K (blue). **(a)** peak particle concentration reached in the first two hours **(b)** time required to reach half the peak particle concentration shown in frame (a).

Fig. 11. Summary of atmospheric box-model calculations with T = 287 K and a diurnal IO profile with peak concentrations of 0.5 (red), 1.0 (black), 3.0 (blue), and 5.0 (greene) ppt and a variable OIO first order loss rate coefficient (see text for details).

Title Page

Abstract | Introduction

Conclusions | References

Tables | Figures

◄◄ | ►►

◄ | ►

Back | Close

Full Screen / Esc

Print Version

Interactive Discussion
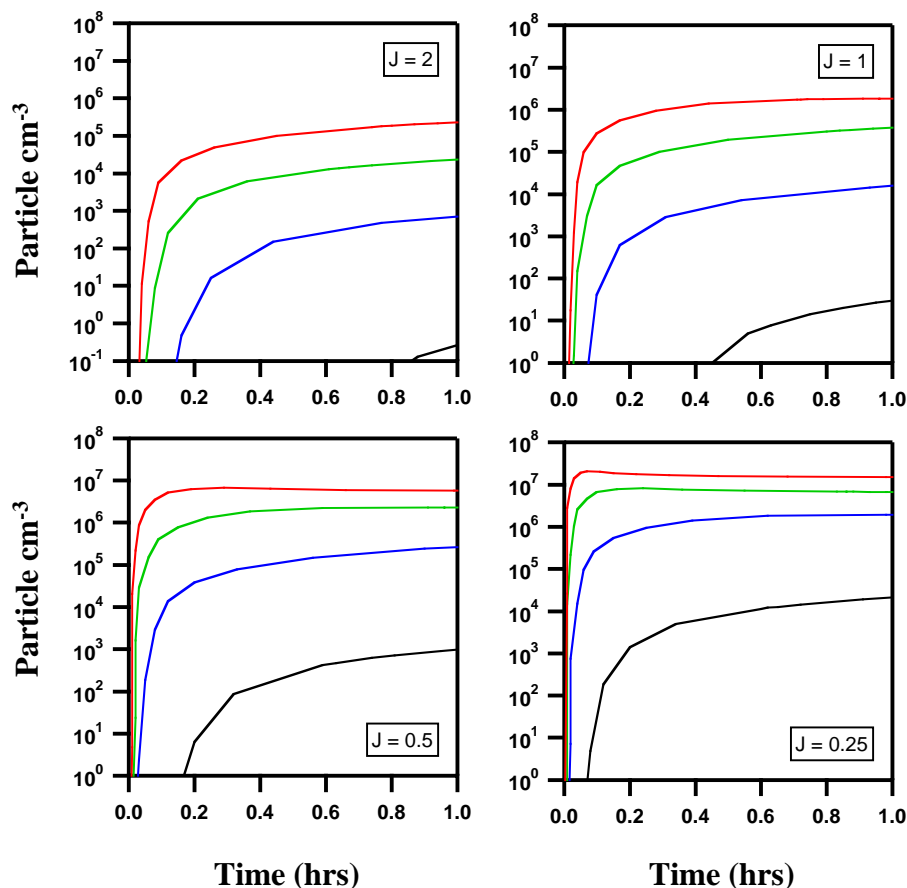
Fig. 12. Aerosol model calculations of particle production (> 3 nm dia., T = 287 K) with IO steady state concentrations of 50 ppt (black), 100 ppt (blue), 150 ppt (green), and 200 ppt (red). Calculations were performed with the thermodynamic parameters determined in this work for OIO photolysis rate coefficients of 2, 1, 0.5, and 0.25 s^{-1} (see text for details).

Title Page

Abstract | Introduction

Conclusions | References

Tables | Figures

|◄ | ►|

◄ | ►

Back | Close

Full Screen / Esc

Print Version

Interactive Discussion